Local structure and spin transition in Fe_2O_3 hematite at high pressure

Andrea Sanson,[1,*] Innokenty Kantor,[2,†] Valerio Cerantola,[2] Tetsuo Irifune,[3] Alberto Carnera,[1] and Sakura Pascarelli[2]

[1]*Department of Physics and Astronomy, University of Padova, Padua, Italy*
[2]*ESRF - European Synchrotron Radiation Facility, Grenoble, France*
[3]*Geodynamic Research Center, University of Ehime, Matsuyama, Japan*

The pressure evolution of the local structure of Fe_2O_3 hematite has been determined by extended x-ray absorption fine structure up to $\sim$79 GPa. Below the phase-transition pressure at $\sim$50 GPa, no increasing of FeO_6 octahedra distortion is observed as pressure is applied. Above the phase transition, an abrupt decrease of the nearest-neighbor Fe-O distance is observed concomitantly with a strong reduction in the FeO_6 distortion. This information on the local structure, used as a test-bench for the different high-pressure forms proposed in the literature, suggests that the orthorhombic structure with space group $Aba2$, recently proposed by Bykova *et al.* [Nat. Commun. **7**, 10661 (2016)], is the most probable, but puts into question the presence of the $P21/n$ form in the pressure range 54–67 GPa. Finally, the crossover from Fe high-spin to low-spin states with pressure increase has been monitored from the pre-edge region of the Fe K-edge absorption spectra. Its "simultaneous" comparison with the local structural changes allows us to conclude that it is the electronic transition that drives the structural transition and not vice versa.

I. INTRODUCTION

The high-pressure behavior of hematite (α-Fe_2O_3) has raised much debate in the scientific community over the past decades. At ambient conditions, hematite crystallizes in the rhombohedral corundum-type structure, space group $R\bar{3}c$, and is a wide-band antiferromagnetic insulator. By increasing pressure at room temperature, the corundum structure of hematite is progressively distorted and, above $\sim$50 GPa, a series of physical changes occur [1–11]: the unit cell volume drops down by about 10%, the crystal symmetry changes completely, the electrical resistivity decreases drastically due to the breakdown of the d-electron correlation (Mott insulator-metal transition), the magnetic moments collapse [transition of iron ions from high-spin (HS) to low-spin (LS) state], and the long-range magnetic order disappears. Besides being interesting from the viewpoint of solid-state physics, the phenomena are also important in geophysics for modeling materials behavior in deep Earth's mantle [12–16].

Despite the many experimental and theoretical studies that have been conducted on this issue, several aspects still remain controversial and unsolved. From the structural point of view, it was initially proposed that the high-pressure (HP) form of Fe_2O_3 was a $GdFeO_3$-type orthorhombic perovskite, containing two different Fe sites with different coordination numbers and characterized by unequal valence states, i.e., Fe^{2+} and Fe^{4+} [17–19]. But a few years later, further investigations established that the HP phase of Fe_2O_3 is a nonmagnetic metallic phase with a single Fe^{3+} cation site, and identified as the distorted Rh_2O_3-II structure [4–6]. In contrast, a very recent synchrotron x-ray single-crystal diffraction study [20,21] proposes that, in the mixed state above 50 GPa, Fe_2O_3 forms a novel monoclinic phase with space group $P2_1/n$ (indexed as distorted perovskite $P\bar{1}$ in Ref. [20]) and, above 67 GPa,

compression triggers the transition to a different HP phase with orthorhombic unit cell and space group $Aba2$. Another important and controversial point refers to the nature of the phase transition at $\sim$50 GPa: is it the structural transition that drives the electronic transition or vice versa? Some authors stated that the structural transition precedes the change in the electronic properties of Fe_2O_3 [2,3], while other authors proposed the opposite scenario [5–9]. Different theoretical approaches lead to different and controversial results.

All these unsolved issues stimulate new high pressure studies of hematite by means of other techniques. One of these is extended x-ray absorption fine structure (EXAFS) spectroscopy that, thanks to its selectivity to atomic species and insensitivity to long range order, is a powerful tool for the study of local structure and electronic properties of solids [22]. However, many difficulties are associated with conducting EXAFS studies at high pressure, due to the strong absorption of the diamond anvils at low x-ray energies (the Fe K edge is at 7.1 keV), and due to intrinsic limitations to the measurable k range for EXAFS because of Bragg diffraction from the diamonds. In this study, Fe K-edge energy dispersive EXAFS measurements have been conducted on Fe_2O_3 under pressures up to $\sim$79 GPa (and then decompressing up to $\sim$19 GPa) at the ID24 XAS beamline of the European Synchrotron Radiation Facility (ESRF) in Grenoble [23]. The recent developments on this beamline, together with the availability of nanodiamond anvils [24], offer the possibility to reach a larger k range (up to about 10 Å^{-1} in the present study) at very high pressures [25,26].

The paper is organized as follows: experimental and data analysis details are given in Sec. II, Secs. III and IV are dedicated to the structural and electronic transitions, respectively, and Sec. V to the conclusions.

---

*Corresponding author: andrea.sanson@unipd.it
†Current address: Technical University of Denmark, Fysikvej, Lyngby, Denmark.

II. EXPERIMENTAL AND DATA ANALYSIS DETAILS

Fe K-edge energy dispersive EXAFS measurements have been performed at the ID24 XAS beamline of ESRF [23].
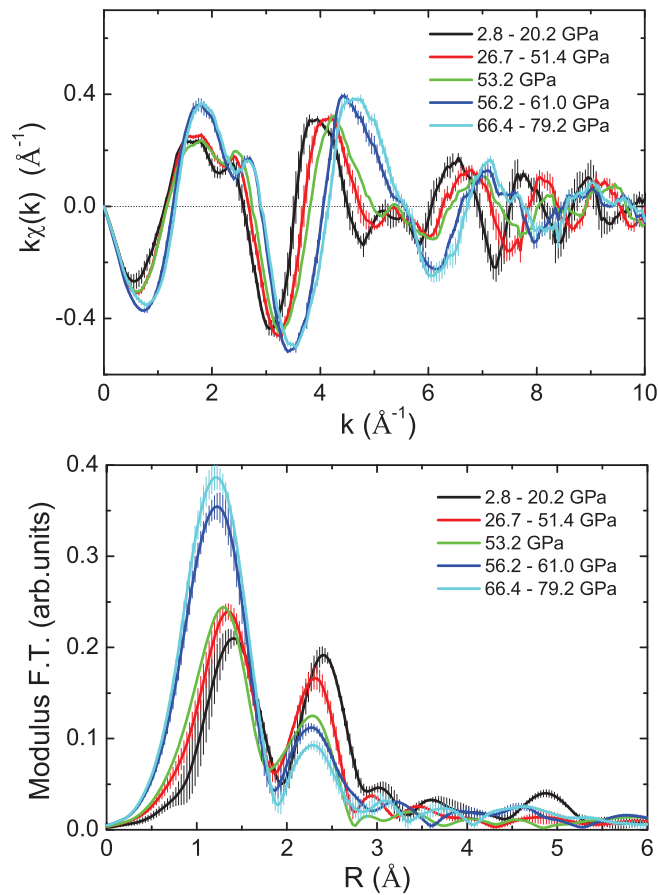
FIG. 1. Fe *K*-edge EXAFS signals of Fe_2O_3 under pressure (top panel) and corresponding Fourier transform (bottom panel). For the sake of clarity, we show the averages of the spectra over the pressure ranges specified in the insets. The vertical bars indicate the corresponding standard deviation.
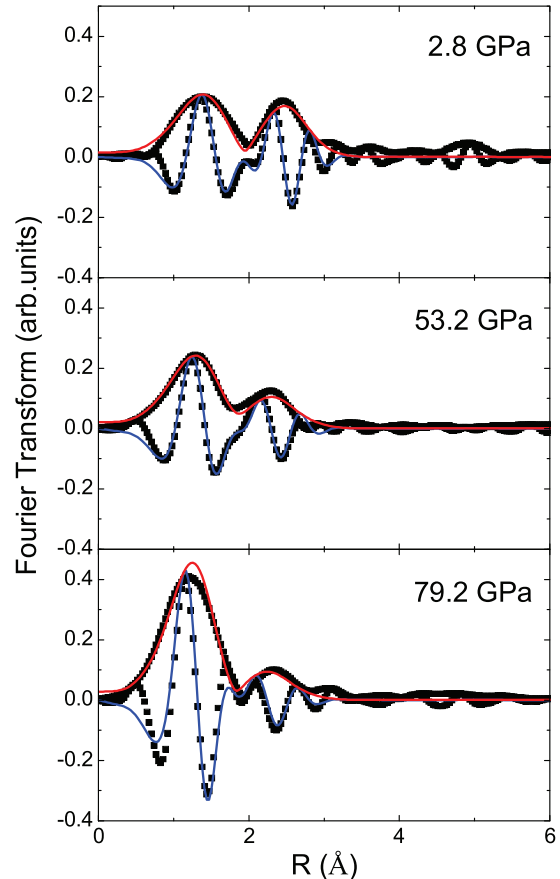

FIG. 2. Modulus and imaginary part of the Fourier transform (black symbols) and best-fitting simulation of the first and second peaks (solid lines) at selected pressures (2.8, 53.2, and 79.2 GPa).

Double-slope nanocrystalline anvils of 2 mm thickness with 150/450 μm culet size were used. Fe_2O_3 hematite powder (99.999% pure, purchased from Aldrich Chemical Co.) together with a few ruby spheres were loaded in two membrane driven diamond anvil cells, filled with helium gas to allow for higher hydrostaticity at high pressures. Pressure was estimated using the signal from the rubies. The pressure was gradually increased up to ~79 GPa (compression) and successively decreased down to ~19 GPa (decompression), with steps of about 2–5 GPa. For each pressure, a map of at least nine single spectra were recorded in different positions of the sample and then averaged.

The EXAFS signals, extracted in a conventional way using the AUTOBK code [27], are shown in the top panel of Fig. 1 and display a good quality up to about 10 Å^{-1}. The $k\chi(k)$ weighted EXAFS signals were Fourier transformed (FT) in the interval $k = 2.5$–10 Å^{-1} using a Gaussian window, as shown in the bottom panel of Fig. 1. The first thing we notice is that above ~55 GPa the phase transition has fully taken place. This is evinced from the sharp increase in the first FT peak below ~2 Å and from the decrease in the second FT peak between ~2 and 2.8 Å. According to FEFF calculations [28,29], in the

hematite form at ambient conditions the first FT peak is due to the single scattering from the nearest-neighbor Fe-O distances of the distorted FeO_6 octahedron (three short distances at ~1.94 Å and three long at ~2.12 Å), while the second FT peak is due to the single scattering from the next-nearest-neighbor Fe-Fe distances, i.e., one at ~2.90 Å and three at ~2.97 Å.

The data were fitted in R-space, between 0.3 and 2.8 Å, using using the FEFFIT code [30] (Fig. 2). Backscattering amplitudes and phase shifts for the Fe-O and Fe-Fe atomic pairs in hematite were used. By taking into account the limited k range of the EXAFS signal, that the HP structure of Fe_2O_3 is not well defined and the large number of distances involved, the nearest-neighbor Fe-O distances were assumed to follow one single-peak average distribution. The validity of this assumption was tested in Ref. [31] and is also confirmed by the subsequent agreement with the crystallographic data of hematite. The same assumption was made for the analysis of the next-nearest-neighbor Fe-Fe/O distances (see the Supplemental Material [32]). Therefore, the free fitting parameters were: average distance and Debye-Waller factor (σ^2) for each of the two Fe-O and Fe-Fe/O average distance distributions, as well as S_0^2 (amplitude reduction factor due to intrinsic inelastic effects) and E_0 (edge energy mismatch between theory and experiment). To reduce the uncertainty bars and the scattering of the results as a function of pressure, S_0^2 was calibrated to

0.9 so to have $\sigma^2 \simeq 0.013$ Å^2 for the Fe-O nearest neighbors at ambient conditions as expected in hematite [33], while E_0 was fixed to the average values -9.7 and -12.8 eV below and above the transition, respectively, calculated from a first analysis performed with E_0 left free.

III. LOCAL STRUCTURE TRANSITION

The average Fe-O distance as a function of pressure is shown in the top panel of Fig. 3. The bottom panel of the same figure shows instead the pressure dependence of the variance (σ^2) of the corresponding average distance distribution. As expected, it can be seen that the Fe-O distance progressively decreases with increasing pressure (red squares), and, above ~50 GPa, we observe an abrupt decrease (of about 0.1 Å) which reveals the HP phase transition of Fe$_2$O$_3$. Very interesting is the behavior of σ^2 above the transition, indicating a sharp decrease of the static disorder in the nearest-neighbor Fe-O distances, consistent with a reduction in the distortion of the FeO$_6$ octahedra. No phase transformation is observed at ~67 GPa (at least within our experimental uncertainty) in contrast to Bykova *et al.* [20], who found a reduction in the splitting of x-ray reflections indicating an increase in crystal symmetry ($P2_1/n \rightarrow Aba2$ phase transformation), associated with a small decrease of molar volume. Finally, during decompression, a hysteresis effect is observed across

the phase transition (blue circles in Fig. 3), although we do not have direct evidence that the phase obtained upon decompression is identical to the initial one. Indeed the σ^2 deviates somewhat from that measured upon compression, and this could be linked to different distortion of the FeO$_6$ octahedra.
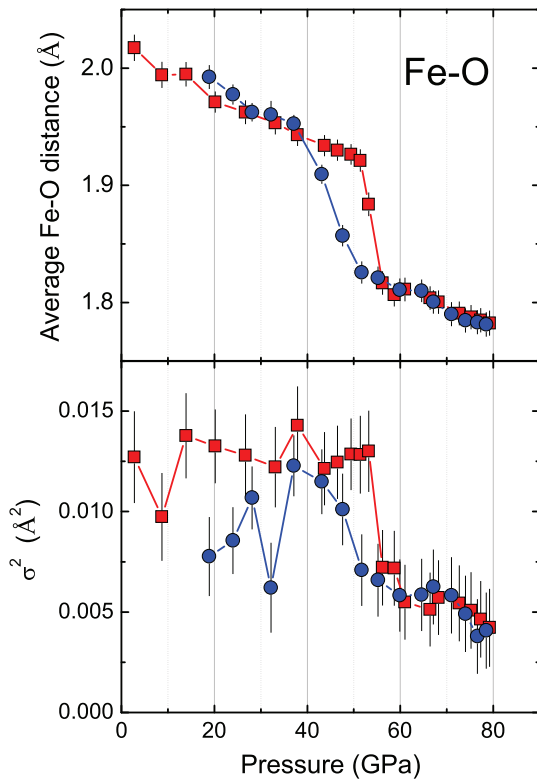

FIG. 3. Pressure dependence of the average Fe-O distance (top panel) and of the variance σ^2 of corresponding Fe-O distribution (bottom panel). Red squares and blue circles refer to compression and decompression, respectively. The solid lines are guide to eyes.
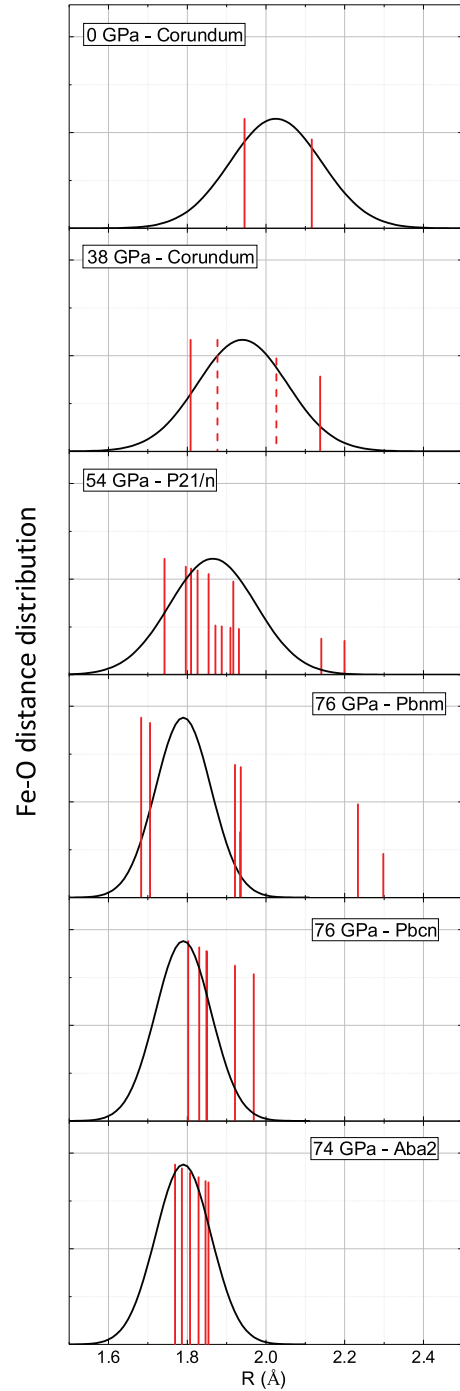

FIG. 4. Fe-O average distributions determined by EXAFS (black-solid lines). The red bars indicate the Fe-O distances according to the HP structures proposed in literature. The red-dashed vertical bars in the second panel from the top are the Fe-O distances of hematite by assuming unchanged the atomic positions in the unit cell, in contrast to Rozenberg *et al.* [6].

Figure 4 provides a visual inspection of the comparison between the Fe-O distance distribution determined by EXAFS (black line) and the Fe-O distances in the different HP forms proposed in the literature [4–6,17–21] (vertical red lines). The EXAFS results are approximated by Gaussian distributions, in accordance to the data reported in Fig. 3. The heights of the vertical red lines were scaled according to the EXAFS amplitude calculated by the FEFF code at 0 K (atoms frozen in their equilibrium positions) and arbitrarily normalized to the height of the Fe-O distributions.

The local structure results of Fig. 4 are summarized in Table I in order to shed light on the controversial HP phase of Fe_2O_3. To have a more honest comparison with EXAFS data, the expected average Fe-O distances and σ^2 of the different HP structures were calculated by weighing the distances according to the EXAFS amplitudes. Note that the EXAFS σ^2 reported in the last column of Table I is the sum of a static contribution σ_{st}^2 due to the presence of Fe-O distances of different lengths, and of a dynamic contribution σ_{din}^2 due to thermal disorder. For the Fe-O nearest neighbors of hematite at ambient conditions, σ_{st}^2 is about 0.007 Å^2, while the average value of σ_{din}^2, determined by temperature-dependent EXAFS measurements and molecular dynamics calculations [33], is about 0.006 Å^2. In the determination of the expected average Fe-O distances and σ^2 of the different HP structures, listed in the second and third columns of Table I, we approximated the dynamic contribution σ_{din}^2 to that of hematite at ambient conditions and weighted the distances according to the EXAFS amplitudes.

At first we consider the HP structure before the transition proposed by Rozenberg and co-workers [6]. According to their refined structural parameters, the resulting average Fe-O distance is in very good agreement with that obtained in the present EXAFS study. However, Rozenberg *et al.* found that pressure induces a progressive distortion of the FeO_6 octahedron, in which the distance gap between short and long Fe-O nearest neighbors progressively increases up to about 0.4 Å, resulting in a progressive increase of the static disorder σ_{st}^2 up to ~0.04 Å^2. This is in sharp contrast with our EXAFS results shown in the bottom panel of Fig. 3, where below the

phase transition σ^2 is constant and ~0.013 Å^2. Accordingly, no further distortion of the FeO_6 octahedra is observed with increasing pressure with respect to ambient conditions. To show this, the average Fe-O structural parameters were calculated from Rozenberg's refinement, for example at 38 GPa (Table I, Corundum A), and the same was done using the lattice parameters of Rozenberg *et al.* but leaving unchanged the atomic positions in the unit cell (Table I, Corundum B). It can be seen that the agreement with the experimental EXAFS data, specifically σ^2, is much better for the latter.

We now consider the HP structures of Fe_2O_3 above the phase transition. For the novel monoclinic phase (space group $P21/n$) proposed by Bykova *et al.* [20,21] in the pressure range 54–67 GPa, only the expected average Fe-O distance is in agreement with that of EXAFS (Table I, 4th row); in contrast, the value of σ^2 is larger and indicates a small, but not negligible, Fe-O distortion, in particular at higher pressures, where the EXAFS σ^2 drops to ~0.005 Å^2, while the expected $P21/n$ σ^2 remains of the order of ~0.015 Å^2. Therefore, the local Fe-O disorder determined by EXAFS is much smaller than that expected for the $P21/n$ phase.

Still more interesting is the comparison to the HP structures above 70 GPa. The local structural parameters of the $GdFeO_3$-type perovskite structure, space group $Pbnm$, are completely at odds with the EXAFS results (Table I, 5th row), independently on whether the Fe-O distances at 2.3 Å are included or not. In particular, the static disorder of the nearest-neighbor Fe-O distribution is too large compared to that measured by EXAFS, therefore, in agreement with previous studies [4–6,15], we can rule out the $GdFeO_3$ form as HP structure of Fe_2O_3. However, we come to the same conclusion also for the distorted Rh_2O_3-II structure, space group $Pbcn$, which was, until recently, the most accepted HP structure for Fe_2O_3 [4–6]. Indeed, from Table I, 6th row, the structural parameters of this phase show a significant discrepancy with the EXAFS results. On the contrary, the best agreement seems to be found for the orthorhombic structure with space group $Aba2$ (Table I, 7th row), the HP structure very recently proposed by Bykova and co-workers [20] on the basis of synchrotron x-ray single-crystal diffraction. We can

TABLE I. Average Fe-O parameters expected for the different HP structures of Fe_2O_3 (left side) and their comparison with the experimental EXAFS results (right side). In order to do a more accurate comparison, the structural parameters were calculated by weighting the respective distances according to their EXAFS scattering amplitudes, while the dynamic contribution to σ^2 was approximated to those of hematite at ambient conditions (see text).

	Expected		EXAFS	
Crystal structure	Fe–O (Å)	$\sigma_{Fe\text{-}O}^2$ (Å^2)	Fe–O (Å)	$\sigma_{Fe\text{-}O}^2$ (Å^2)
Corundum (0 GPa)	2.02	0.013	2.02 ± 0.01	0.013 ± 0.002
Corundum A (38 GPa)[a]	1.94	0.032	1.94 ± 0.01	0.013 ± 0.002
Corundum B (38 GPa)	1.94	0.012	1.94 ± 0.01	0.013 ± 0.002
$P21/n$ (54 GPa)[b]	1.87	0.017	1.87 ± 0.01	0.012 ± 0.002
$Pbnm$ (76 GPa)[a,c]	1.81/1.88	0.020/0.046	1.79 ± 0.01	0.005 ± 0.002
$Pbcn$ (76 GPa)[a]	1.87	0.009	1.79 ± 0.01	0.005 ± 0.002
$Aba2$ (74 GPa)[b]	1.81	0.007	1.79 ± 0.01	0.005 ± 0.002

[a]Crystal cell from Ref. [6].

[b]From Refs. [20,21].

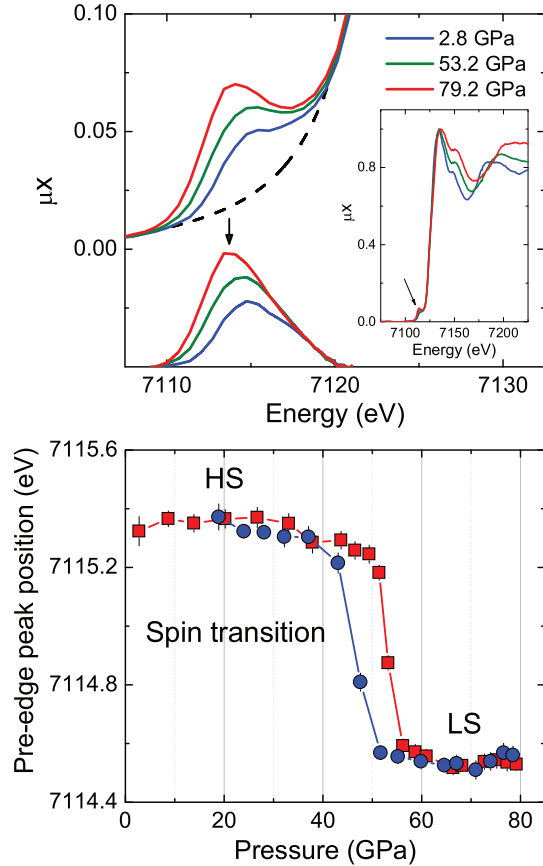[c]The two set of values were obtained by neglecting or including the Fe-O distances at ~2.3 Å, respectively.

FIG. 5. Top panel: Pre-edge peak of the Fe K-edge absorption spectra at selected pressures and corresponding background subtraction. The inset shows the whole absorption spectra. Bottom panel: Fe^{3+} high-spin/low-spin crossover monitored by the average pre-edge peak position as a function of pressure, during compression (red squares) and decompression (blue circles).

conclude that the results on the local structure reported here by EXAFS can be used as a test-bench for proposed or new HP forms of Fe_2O_3.

IV. ELECTRONIC TRANSITION

We now address the electronic spin transition and the controversial issue of the nature of the phase transition of hematite [2,3,5–9], i.e., do the electronic properties of Fe_2O_3 change only after the structural transition with a decrease in volume and a change in the lattice symmetry, or vice versa? In this regard, the evolution of the Fe $3d$ electronic structure vs pressure can be investigated from the pre-edge region of the Fe K-edge absorption spectrum (top panel of Fig. 5), since this pre-edge feature is sensitive to the t_{2g} and e_g components of the $3d$ band through hybridization effects [11,34], and therefore is directly connected to the population of the HS and LS states. After normalization and background subtraction of absorption spectra (top panel of Fig. 5), the average position of the pre-edge peak was determined and plotted as a function of pressure (bottom panel of Fig. 5): in this way we monitor the crossover from HS to LS states with pressure increase and vice versa. Since it is known that Fe ions in Fe_2O_3 at ambient
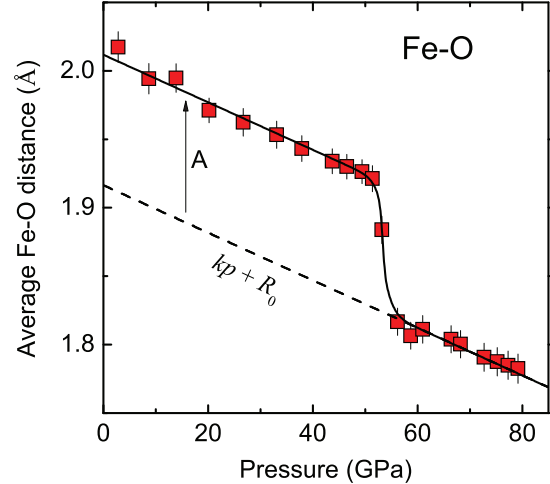

FIG. 6. Fe-O distance during compression (red squares) and corresponding best-fit curve (solid line) using Eq. (1). The dashed line shows the contribution due to the mere effect of pressure increase which must be subtracted to calculate the corresponding phase-transition fraction.

conditions are all in the HS state and above 70 GPa are all in the LS state [20], we can deduce that the pre-edge peak position in the bottom panel of Fig. 5 monitors the complete spin transition from 100% Fe-HS at 0 GPa to 100% Fe-LS at 79 GPa.

The "simultaneous" measurement of the structural transition (Fig. 3) and of the electronic transition (Fig. 5), i.e., probed truly simultaneously and from the same portion of the sample, is fundamental to overcome the uncertainty due to different hydrostatic conditions and different measured volume, and allows addressing questions related to the interplay between structural and electronic/magnetic degrees of freedom in Fe_2O_3, as previously demonstrated for pure Fe [35]. In this regard, let us calculate the "phase-transition fraction" as follows.

First, we consider the structural phase-transition fraction. The pressure evolution of the Fe-O distance (top panel of Fig. 3 and also reported in Fig. 6) was fitted by the function

$$R(p) = \frac{A}{e^{p-p_0} + 1} + kp + R_0, \qquad (1)$$

where the first term is of the Fermi-Dirac form, the second linear term kp takes into account the Fe-O decrease/increase due to the mere effect of compression/decompression, and R_0 is an offset parameter. Figure 6 reports the result of the best fit (solid black line) of the experimental Fe-O distance during compression, $R_{\text{expt}}(p)$. We then use this function to extract the structural phase transition fraction (in percent) as follows:

$$100\left[1 - \frac{R_{\text{expt}}(p) - kp - R_0}{A}\right]. \qquad (2)$$

By using the same fitting procedure, the structural phase-transition fraction during decompression was calculated as

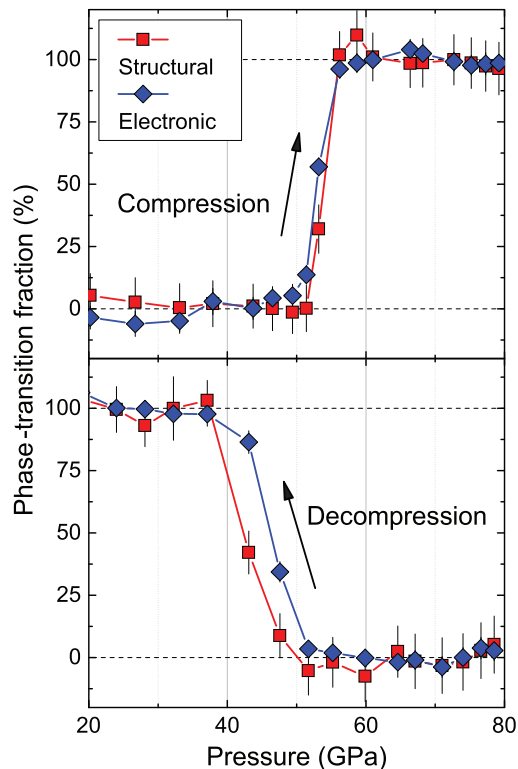$$100\left[\frac{R'_{\text{expt}}(p) - kp - R_0}{A}\right], \qquad (3)$$

FIG. 7. Phase-transition fraction (in percent) during compression (top panel) and decompression (bottom panel). Red squares refer to the structural transition and blue diamonds to the electronic transition. In both cases, the electronic transition precedes the structural transition.

where here $R'_{\text{expt}}(p)$ is the pressure evolution of the Fe-O distance during decompression (blue circles in the top panel of Fig. 3). With the same procedure we have calculated the electronic phase-transition fraction, both in compression and decompression, with the only difference that k was set to zero assuming that the HS/LS population does not vary linearly with pressure.

As a result, Fig. 7 shows the evolution of the phase-transition fraction, both structural and electronic, during compression (top panel) and decompression (bottom panel). During compression, in the mixed HS/LS state at about 53 GPa, the electronic transition is ~60% completed (blue diamonds in the top panel of Fig. 7), while the structural transition (red squares) is only ~30% completed. As a result, we can deduce that the HP structural transition occurs only after the electronic transition to the low-spin phase. Further confirmation of this finding is given by the data collected during decompression. At about 48 and 43 GPa, the LS to HS transition is completed at ~35% and ~85%, respectively (blue diamonds in the bottom panel of Fig. 7), while the structural transition (red squares) is only completed at ~10% and ~40%, respectively. This shows again that the electronic transition actually precedes the structural transition, and leads to the following description of the HP transition of Fe_2O_3: (i) volume and bond distances decrease with pressure until a "volume threshold" value is reached at ~50 GPa, in which the low-spin phase is more stable as predicted by some theoretical calculations [8,9,36]. The

spin crossover transition from HS to LS states is thus activated. (ii) The majority of the HS to LS transition occurs between ~50 and 55 GPa. In this pressure interval, the sample enters into a phase characterized by Fe^{3+} ions in the mixed HS/LS state. The crystal structure is initially unchanged, but a further increase in pressure triggers the Fe^{3+} ions into the stable LS phase, thus causing the structural transition and volume collapse (LS Fe atomic radius becomes ~0.1 Å shorter than that of HS Fe [37]) as a consequence of emptying of the antibonding bands in the LS phase and corresponding strengthening of the Fe-O bonds [8]. (iii) Above ~55 GPa the Fe^{3+} ions are all (or almost) in the LS state, and bond distances and volume continue to decrease as a mere effect of pressure increase.

The major finding on the relationship between the electronic and structural transition of the present work agrees with many previous studies [5–9], but contradicts the conclusions of previous work by Badro *et al.* [2], where a combination of x-ray powder diffraction and x-ray emission spectroscopy was used to probe crystal structure and spin state of Fe_2O_3. We believe that the major reason for this discrepancy resides in the experimental design. Our study demonstrates that a true simultaneous probe of structural and electronic properties is crucial for revealing correlations between them. Using the same x-ray beam to probe both guarantees that the probed sample volumes coincide. Otherwise the combination of small samples and pressure or stress inhomogeneities, typical for diamond anvil cell experiments, can lead to wrong conclusions. In the earlier study [2] the measurements of structural and electronic states were not simultaneous and not necessarily from the same sample portion. This would also explain why the x-ray diffraction patterns of the quenched metastable phase and of the 10 h relaxed phase are not identical (Fig. 2 from the original work [2]).

Before concluding, let us point out that, according to Bykova *et al.* [20], the $P21/n$ phase ranges from ~54 to 67 GPa; the HS/LS ratio, equal to 1 after the transition at 54 GPa, is strongly affected upon compression and only LS states survive at 67 GPa. In contrast, we find that Fe atoms are practically all in the LS state already at 56 GPa (top panel of Fig. 7). In addition, our EXAFS analysis reveals that the local Fe-O disorder above 54 GPa is considerably lower than expected in the $P21/n$ phase. Therefore, according to our study, we may infer that the $P21/n$ phase, if really present, occurs in the shorter interval ~50–55 GPa.

V. CONCLUSIONS

In this work we first studied the local structure of Fe_2O_3 hematite under high pressure. Below the phase transition, no increase in the FeO_6 octahedra distortion is observed as pressure is applied, in contrast to Rozenberg *et al.* [6]. More importantly, an abrupt decrease in the nearest-neighbor Fe-O distance is observed at ~50 GPa. Concomitantly, we observe a peculiar decrease of the nearest-neighbor Fe-O static disorder, indicating a reduction in the FeO_6 distortion.

The present EXAFS results represent an excellent test-bench for proposed or new HP forms of Fe_2O_3. Comparison to the different HP phases proposed in the literature rules out both the $GdFeO_3$-type orthorhombic perovskite form and the distorted Rh_2O_3-II structure, and rather suggests that

the orthorhombic structure with space group *Aba*2, recently proposed by Bykova *et al.* [20], is the most appropriate among those reported in literature. Moreover, we put into question the real presence of the $P21/n$ phase in the whole pressure range 54–67 GPa, because its local Fe-O disorder is incompatible with that measured by EXAFS.

Finally, the pressure-induced Fe^{3+} high-spin to low-spin transition has been monitored from the pre-edge peak of the Fe K-edge absorption spectra. The simultaneous comparison with the pressure evolution of the local structural transition determined by EXAFS, extracted from the same spectrum, allows us to conclude that it is the electronic transition that drives the structural transition and not vice versa, thus solving the long standing controversy on the nature of the phase transition. The details of the dynamics of this phase transition, in particular the nature of the observed mixed HS/LS phase, call for further theoretical and experimental investigations.

[1] E. Knittle and R. Jeanloz, Solid State Commun. **58**, 129 (1986).

[2] J. Badro, G. Fiquet, V. V. Struzhkin, M. Somayazulu, H.-K. Mao, G. Shen, and T. Le Bihan, Phys. Rev. Lett. **89**, 205504 (2002).

[3] J.-F. Lin, J. S. Tse, E. E. Alp, J. Zhao, M. Lerche, W. Sturhahn, Y. Xiao, and P. Chow, Phys. Rev. B **84**, 064424 (2011).

[4] H. Liu, W. A. Caldwell, L. R. Benedetti, W. Panero, and R. Jeanloz, Phys. Chem. Minerals **30**, 582 (2003).

[5] M. P. Pasternak, G. Kh. Rozenberg, G. Yu. Machavariani, O. Naaman, R. D. Taylor, and R. Jeanloz, Phys. Rev. Lett. **82**, 4663 (1999).

[6] G. Kh. Rozenberg, L. S. Dubrovinsky, M. P. Pasternak, O. Naaman, T. Le Bihan, and R. Ahuja, Phys. Rev. B **65**, 064112 (2002).

[7] V. Kozhevnikov, A. V. Lukoyanov, V. I. Anisimov, and M. A. Korotin, J. Exp. Theor. Phys. **105**, 1035 (2007).

[8] J. Kuneš, Dm. M. Korotin, M. A. Korotin, V. I. Anisimov, and P. Werner, Phys. Rev. Lett. **102**, 146402 (2009).

[9] D. B. Ghosh and S. de Gironcoli, arXiv:0905.3414.

[10] N. C. Wilson and S. P. Russo, Phys. Rev. B **79**, 094113 (2009).

[11] S. Wang, W. L. Mao, A. P. Sorini, C. C. Chen, T. P. Devereaux, Y. Ding, Y. Xiao, P. Chow, N. Hiraoka, H. Ishii, Y. Q. Cai, and C. C. Kao, Phys. Rev. B **82**, 144428 (2010).

[12] R. C. Liebermann and E. Schreiber, J. Geophys. Res. **73**, 6585 (1968).

[13] K.-I. Kondo, T. Mashimo, and A. Sawaoka, J. Geophys. Res. **85**, 977 (1980).

[14] T. Yagi and S. Akimoto, *High-Pressure Research in Geophysics* (Kluwer Academic, Tokyo, 1982).

[15] S.-H. Shim and T. S. Duffy, Amer. Mineral. **87**, 318 (2002).

[16] S.-H. Shim, A. Bengtson, D. Morgan, W. Sturhahn, K. Catalli, J. Zhao, M. Lerche, and V. Prakapenka, Proc. Natl. Acad. Sci. **106**, 5508 (2009).

[17] T. Suzuki, T. Yagi, S. Akimoto, A. Ito, S. Morimoto, and T. Syono, in *Solid State Physics under Pressure*, edited by S. Minomura (KTK Scientific, Tokyo, 1985), p. 149.

[18] J. Staun Olsen, C. S. G. Cousins, L. Gerward, H. Jhans, and B. J. Sheldon, Phys. Scripta **43**, 327 (1991).

[19] Y. Syono, A. Ito, S. Morimoto, S. Suzuki, T. Yagi, and S. Akimoto, Solid State Commun. **50**, 97 (1984).

[20] E. Bykova, L. Dubrovinsky, N. Dubrovinskaia, M. Bykov, C. McCammon, S. V. Ovsyannikov, H.-P. Liermann, I. Kupenko, A. I. Chumakov, R. Rüffer, M. Hanfland, and V. Prakapenka, Nat. Commun. **7**, 10661 (2016).

[21] E. Bykova, M. Bykov, V. Prakapenka, Z. Konpková, H.-P. Liermann, N. Dubrovinskaia, and L. Dubrovinsky, High Pressure Res. **33**, 534 (2013).

[22] A. E. Stern, *X-Ray Absorption: Principles, Applications, Techniques of EXAFS, SEXAFS and XANES* (Wiley, New York, 1988).

[23] S. Pascarelli *et al.*, J. Synchrotron Rad. **23**, 353 (2016).

[24] T. Irifune, A. Kurio, S. Sakamoto, T. Inoue, and H. Sumiya, Nature (London) **421**, 599 (2003).

[25] M. Baldini, W. Yang, G. Aquilanti, L. Zhang, Y. Ding, S. Pascarelli, and W. L. Mao, Phys. Rev. B **84**, 014111 (2011).

[26] R. Torchio, O. Mathon, and S. Pascarelli, Coord. Chem. Rev. **277-278**, 80 (2014).

[27] M. Newville, P. Līviņški, Y. Yacoby, J. J. Rehr, and E. A. Stern, Phys. Rev. B **47**, 14126 (1993).

[28] A. L. Ankudinov, B. Ravel, J. J. Rehr, and S. D. Conradson, Phys. Rev. B **58**, 7565 (1998).

[29] J. J. Rehr, J. J. Kas, F. D. Vila, M. P. Prange, and K. Jorissen, Phys. Chem. Chem. Phys. **12**, 5503 (2010).

[30] M. Newville, B. Ravel, J. J. Rehr, E. Stern, and Y. Yacoby, Physica B **208-209**, 154 (1995).

[31] A. Sanson, A. Zaltron, N. Argiolas, C. Sada, M. Bazzan, W. G. Schmidt, and S. Sanna, Phys. Rev. B **91**, 094109 (2015).

[32] See Supplemental Material at http://link.aps.org/supplemental/10.1103/PhysRevB.94.014112 for results and discussion on the next-nearest-neighbor Fe-Fe/O distances.

[33] A. Sanson, O. Mathon, and S. Pascarelli, J. Chem. Phys. **140**, 224504 (2014).

[34] W. A. Caliebe, C.-C. Kao, J. B. Hastings, M. Taguchi, A. Kotani, T. Uozumi, and F. M. F. de Groot, Phys. Rev. B **58**, 13452 (1998).

[35] O. Mathon, F. Baudelet, J. P. Itié, A. Polian, M. d'Astuto, J. C. Chervin, and S. Pascarelli, Phys. Rev. Lett. **93**, 255503 (2004).

[36] G. Rollmann, A. Rohrbach, P. Entel, and J. Hafner, Phys. Rev. B **69**, 165107 (2004).

[37] R. D. Shannon, Acta Crystallogr. Sect. A **32**, 751 (1976).